Supplementary Information

In vivo screening of hydrogel library using cellular barcoding identifies biomaterials that mitigate host immune responses and fibrosis

Sudip Mukherjee[*,1], Boram Kim[*,1], Lauren Y. Cheng[*,1], Michael David Doerfert[1], Jiaming Li[1], Andrea Hernandez[1], Lily Liang[1], Maria Ruocco[1], Peter D. Rios[2], Sofia Ghani[2], Ira Joshi[2], Douglas Isa[2], Trisha Ray[3], Tanguy Terlier[4], Ping Song[1], Roberto N. Miranda[5], Jose Oberholzer[2], David Yu Zhang[#,1], Omid Veiseh[#,1]

[1]Department of Bioengineering, Rice University, 6500 Main Street, Houston, TX, USA
[2]CellTrans, Inc., Chicago, IL, USA
[3]Department of Biomedical Engineering, Cornell University, Weill Hall, Ithaca, NY, USA
[4]SIMS laboratory, Shared Equipment Authority, Rice University, 6500 Main Street, Houston, TX, USA
[5]Department of Hematopathology, Division of Pathology/Lab Medicine, The University of Texas MD Anderson Cancer Center, Houston, TX, USA

[*]: Equal Contributing authors
[#]: Corresponding authors
Email address: D.Y.Z <genomic.dave@gmail.com>, O.V. <omid.veiseh@rice.edu>

Table of Contents

Supplementary Results

Synthesis of small molecules and modified alginates

Synthesis of B1-A51 amine:

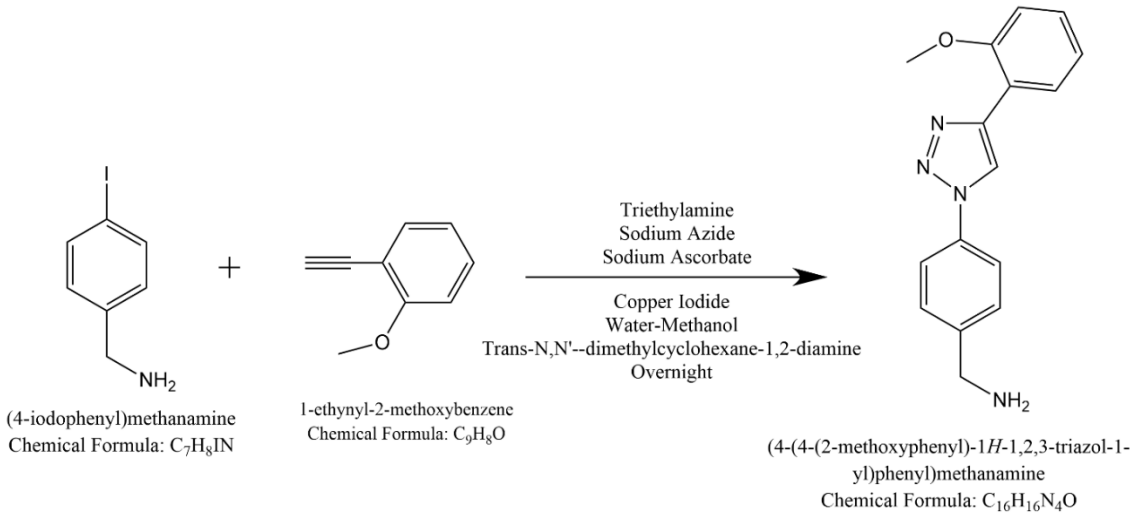

Scheme 1. Schematic representation for the synthesis of B1-A51.

Mass and NMR data

^{1}H (600 MHz; $CDCl_3$): 3.63 (s, 3H, CH3-O-C), 4.01 (s, 2H, NH2-CH2-CH2), 7.05 (s, 1H, -O-benzene), 7.17 (m, 2H, aromatic), 7.52 (m, 2H, aromatic), 7.79 (s, 1H, triazole)

^{13}C (600 MHz; $CDCl_3$): 46.5 (NH2CH2), 56.8 (CH3-O-CH2), 111.4 (CH3-O-CH2-C(aromatic)), 121.6 (CH aromatic), 122.7 (CH triazole), 128.4(CH aromatic), 135.8 (Cq-N aromatic), 144.9 (Cq-C aromatic), 146.9 (C triazole), 157.6 (O-C(aromatic))

ESI: M+1 = 281.1.

Synthesis of B1-A51 alginate:

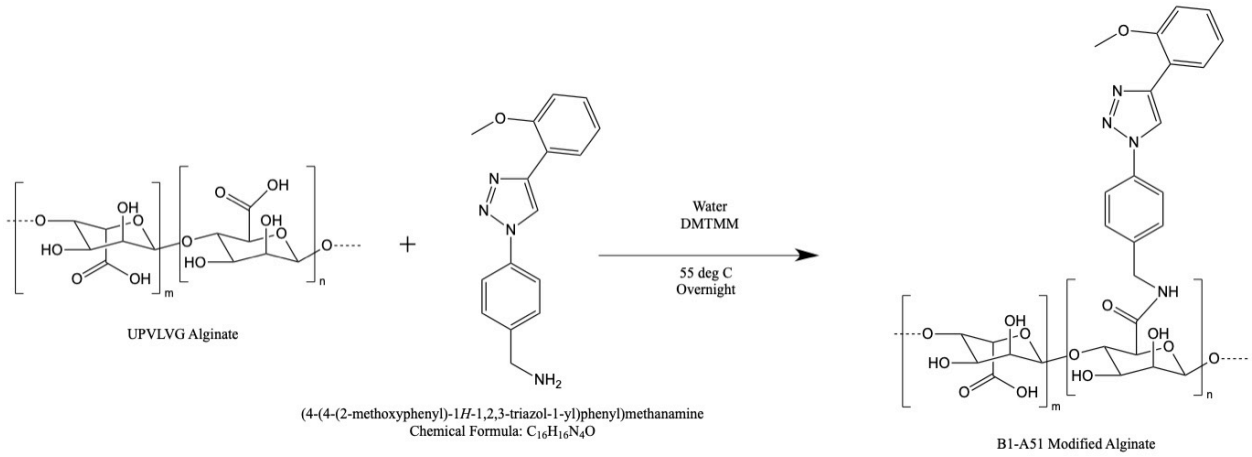

Scheme 2. Schematic representation for the modification of alginate with B1-A51.

NMR data1 H (600 MHz; CDCl3): 3.23-3.45 (m, alginate protons), 3.72 (s, 2H, C-H2C-O), 3.75 (s, 3H, CH3-O), 3.8–5.2 (m, alginate protons), 4.59 (s, 1H, C-CH-O), 4.61 (s, 2H, C-CH2-O), 7.18 (s, 1H, O-CH aromatic), 7.32 (s, 2H, aromatic), 7.67 (s, 2H, aromatic), 8.04 (s, 1H, triazole).
Elemental: C: 34.75%, H: 8.55%, N: 3.56%.

Synthesis of Z1-A34 amine:

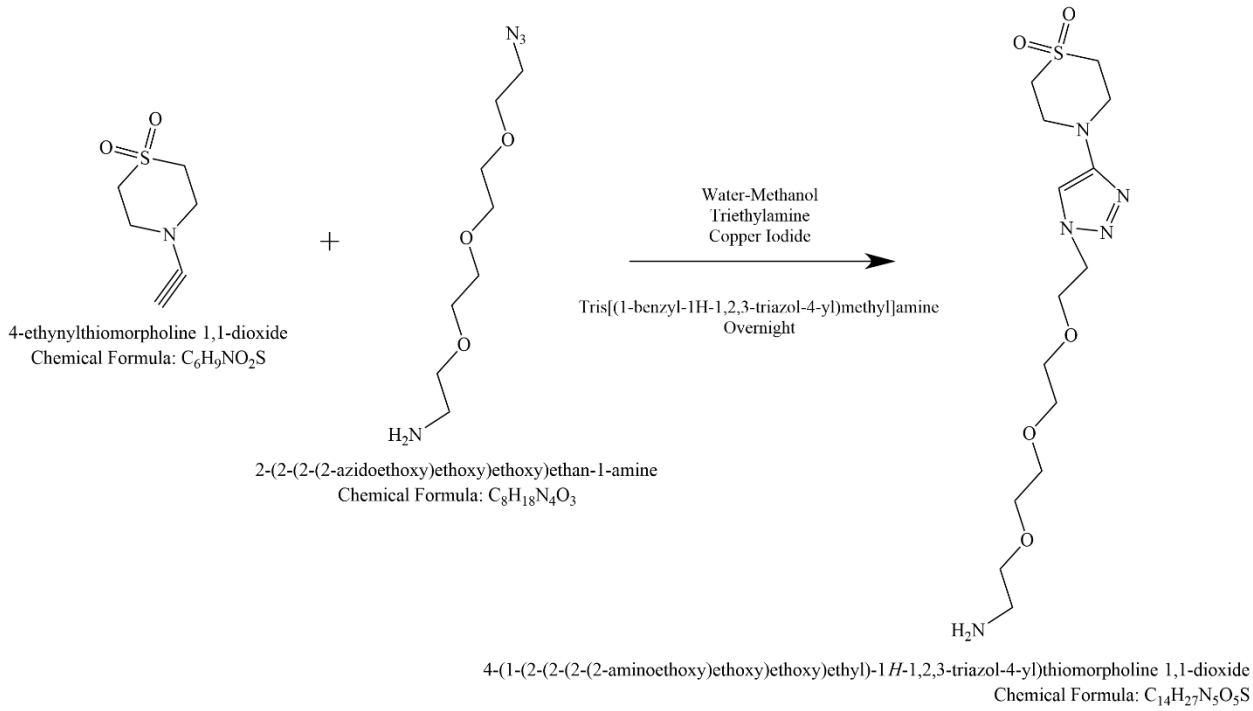

Scheme 3. Schematic representation for the synthesis of Z1-A34.

Mass and NMR data

^{1}H (600 MHz; $CDCl_3$): 2.87 (s, 2H, NH_2-CH_2-CH_2-O), 3.05 (m, 8H, N-CH_2-CH_2-S), 3.51 (t, 2H, NH_2-CH_2), 3.61 (m, 8H, PEG) 3.81 (s, 2H, -CH_2-Triazole), 3.89 (t, 2H, N-CH_2-CH_2-O), 4.55 (t, 2H, N-CH_2-CH_2-O), 7.51 (s, 2H, aromatic), 7.68 (s, 1H, triazole).

^{13}C (600 MHz; $CDCl_3$): 41.74 (NH_2-CH_2), 50.42 (N-CH_2), 50.56 (N-CH_2 Thiomorpholine) 51.52 (S-CH_2 Thiomorpholine) 52.2 (Thiomorpholine-CH_2-Triazole), 69.54-73.14 (m, PEG), 124.10 (CH triazole), 143.32 (C triazole).

ESI MS: $[M+H^+]$ = 392.1939

Synthesis of Z1-A34 alginate:

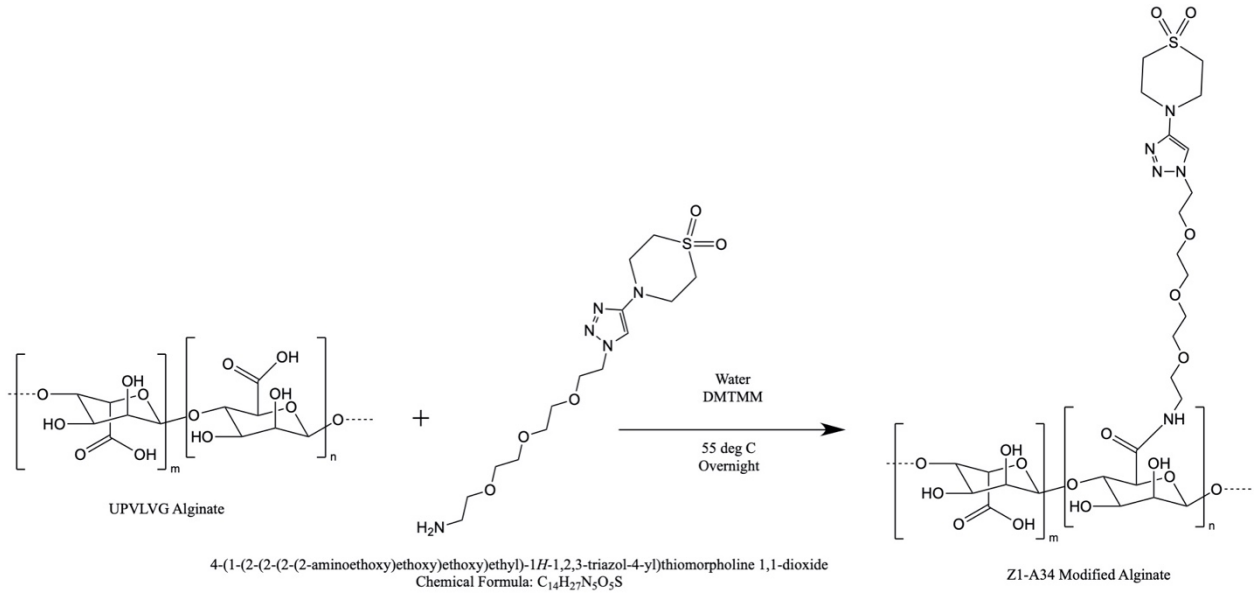

Scheme 4. Schematic representation for the modification of alginate with Z1-A34.

NMR data1 H (600 MHz; D_2O): 2.95 (s, 4H, N-CH_2-CH_2-S), 3.05-3.34 (m, alginate protons), 3.56 (s, 4H, N-CH_2-CH_2-S), 3.48-3.71 (16H, m, ethoxy), 3.65–5.32 (m, alginate protons), 8.08 (1H, s, triazole).
Elemental: C: 35.67%, H: 4.34%, N: 5.08%, O: 33.50%.

Synthesis of Z4-A10 amine:

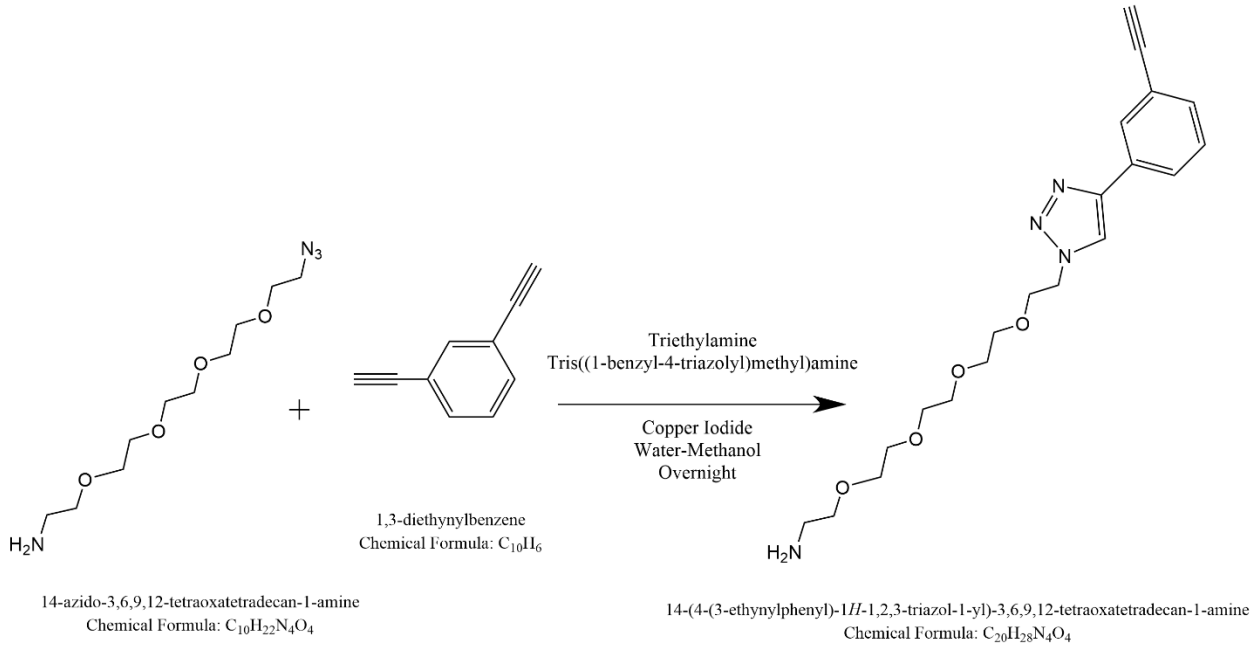

Scheme 5. Schematic representation for the synthesis of Z4-A10.

Mass and NMR data

^{1}H (600 MHz; $CDCl_3$): 2.93 (s, 2H, NH_2-CH_2-CH_2-O), 3.15 (s, H, alkyne), 3.47 (t, 2H, NH_2-CH_2), 3.65(m, 8H, PEG) 3.86 (s, 2H, CH_2-triazole), 3.89 (t, 2H, N-CH_2-CH_2-O), 4.55 (t, 2H, N-CH_2-CH_2-O), 7.69 (s, 1H, triazole), 7.79 (s, 2H, aromatic).

^{13}C (600 MHz; CDCl3): 40.7 (NH2CH2), 51.8 (N-CH2-C), 69.2 (N-C-CH2–O), 71.5 (C-CH2–O), 73.2 (N-CH2-CH2–O), 82.1 (alkyne), 119.6 (H_2C=C), 122.6 (CH aromatic), 127.7 (CH aromatic), 129.5 (CH aromatic), 130.6 (CH aromatic), 132.4 (CH aromatic), 133.4 (C triazole), 139.7 (CH aromatic), 147.9 (1-ethylyne), 166.5 (C, NH-C=O).

ESI MS: $[M+H^+]$ = 389.2080

Synthesis of Z4-A10 alginate:

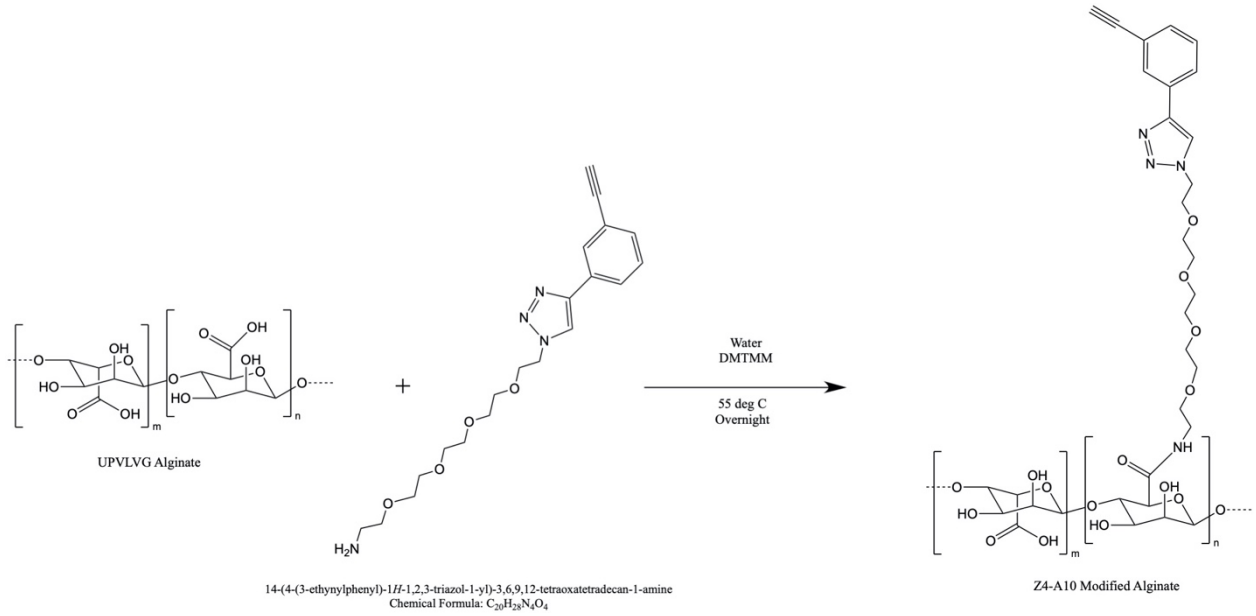

Scheme 6. Schematic representation for the modification of alginate with Z4-A10.

NMR: 1H (600 MHz; D_2O): 3.12 (s, alkyne), 3.17-3.40 (m, alginate protons), 3.50-3.70 (m, 16H, ethoxy), 3.7–5.2 (m, alginate protons), 8.08 (s, 1H, triazole)

Elemental: C: 40.45%, H: 5.60%, N: 6.22%.

Synthesis of Z1-A3 amine:

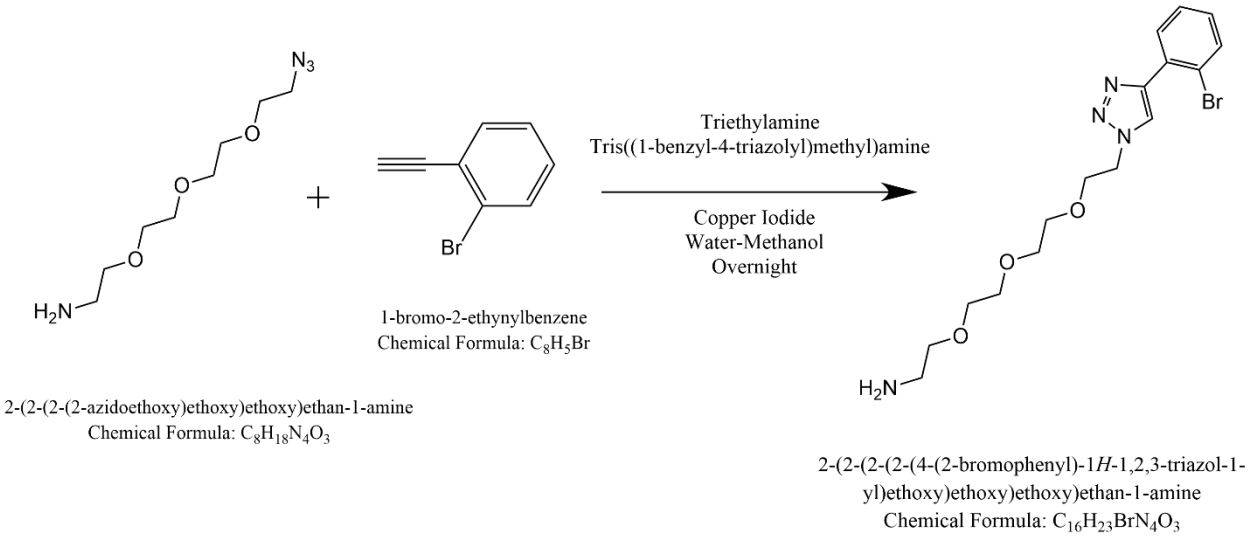

Scheme 7: Schematic representation for the synthesis of Z1-A3.

Mass and NMR data

^{1}H (600 MHz; D_2O): 3.48 (m, 1H, methylene), 3.54 (m, 1H, methylene), 3.91 (s, 1H, NH2-CH2), 4.74 (d, 1H, J= 12Hz, O-CH2-triazole), 4.89 (d, 1H, J=12Hz, O-CH2-triazole), 7.32 (m, 2H, aromatic), 7.54 (m, 2H, aromatic), 7.75 (m, 2H, aromatic), 8.46 (s, 1H, triazole)

^{13}C (600 MHz; D_2O): 40.1 (NH2CH2), 49.9 (N-CH2-C), 67.5 (N-C-CH2–O), 70.1 (C-CH2–O), 72 (N-CH2-CH2–O), 122.2 (CH aromatic), 127.2 (CH aromatic), 130.4 (CH aromatic), 134.1 (C triazole)

ESI: M+1 = 399.1.

Synthesis of Met-Z1-A3:

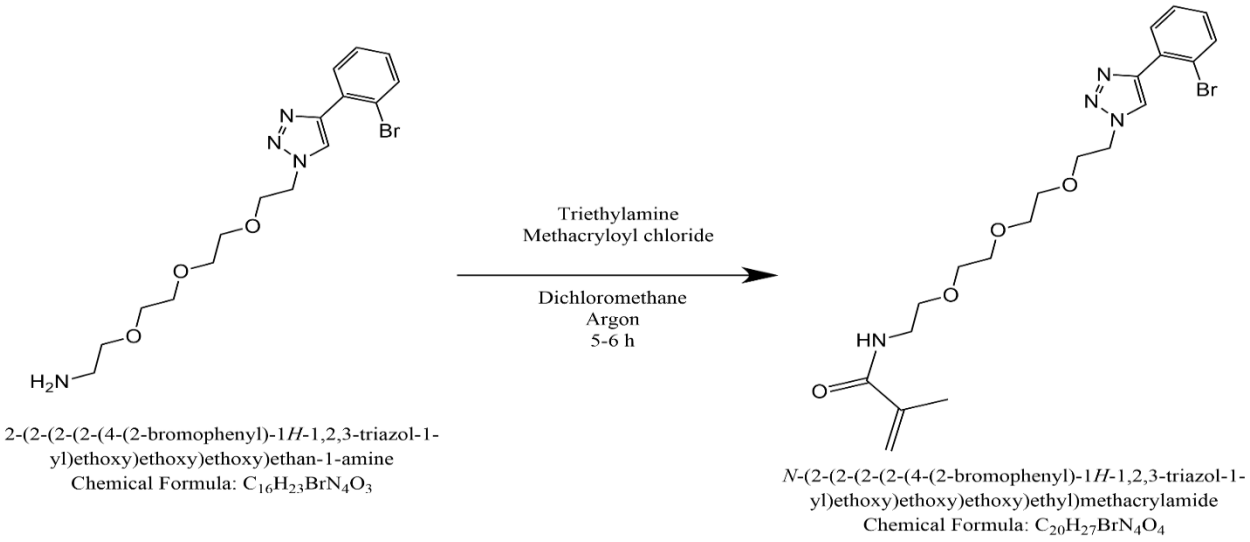

Scheme 8. Schematic representation for the synthesis of Met-Z1-A3.

Mass and NMR data

^{1}H (600 MHz; $CDCl_3$): 1.95 (m, 1H, methyl), 3.53 (m, 1H, methylene), 3.55 (m, 1H, methylene), 3.89 (s, 1H, NH2-CH2), 4.76 (d, 1H, J= 12Hz, O-CH2-triazole), 4.85 (d, 1H, J=12Hz, O-CH2-triazole), 5.28 (1H, 1 ethylene), 5.74 (d, 1H, 1 ethylene), 7.18 (m, 2H, aromatic), 7.52 (m, 2H, aromatic), 7.73 (m, 2H, aromatic), 7.75 (m, 2H, aromatic), 8.42 (s, 1H, triazole)

^{13}C (600 MHz; CDCl3): 18.6 (CH_3), 39.3 (NH2CH2), 50.4 (N-CH2-C), 69.6 (N-C-CH2–O), 70.5 (C-CH2–O), 72 (N-CH2-CH2–O), 119.6 (H_2C=C), 122.2 (CH aromatic), 127.2 (CH aromatic), 129.3 (CH aromatic), 130.58 (CH aromatic), 131.4 (CH aromatic), 133.5 (C triazole), 139.9 (CH aromatic), 145.2 (1-ethylene), 168.38 (C, NH-C=O).

ESI: M+1 = 469.1.

<u>Synthesis of B2-A17 amine:</u>

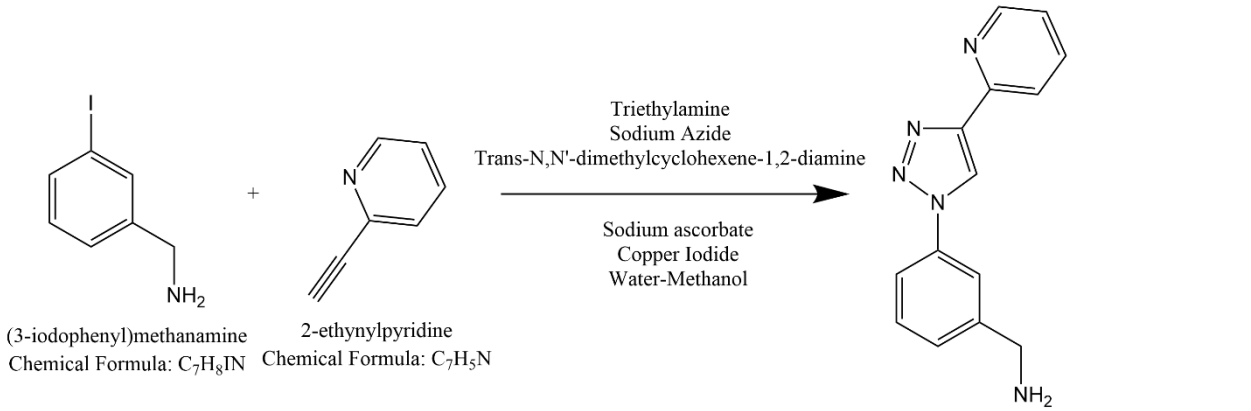

(3-iodophenyl)methanamine
Chemical Formula: C_7H_8IN

2-ethynylpyridine
Chemical Formula: C_7H_5N

(3-(4-(pyridin-2-yl)-1*H*-1,2,3-triazol-1-yl)phenyl)methanamine
Chemical Formula: $C_{14}H_{13}N_5$

Scheme 9. Schematic representation for the synthesis of B2-A27.

Mass and NMR data

^{1}H (600 MHz; DMSO-D6): 4.17 (s, 2H, NH2-CH2-Ph), 7.25 (d, 2H, aromatic), 7.48 (s, 1H, aromatic), 7.52 (s, 2H, aromatic-triazole), 7.87 (s, 1H, aromatic), 7.96 (s, 1H, triazole), 8.25 (s, 1H, aromatic-triazole), 8.59 (s, 2H, amine), 8.65 (s, 1H, aromatic-N).

^{13}C (600 MHz; MeOD):

44.2 (CH2-NH2), 119.6 (CH aromatic), 121.3 (CH aromatic), 123.7 (CH aromatic), 127.8 (CH aromatic), 129.4 (CH triazole), 137.4 (Cq-N aromatic), 142.3 (Cq-C aromatic), 148.9 (C-N aromatic), 151.2 (C-aromatic).

ESI: M+1 = 252.1545

Synthesis of Met-B2-A17:

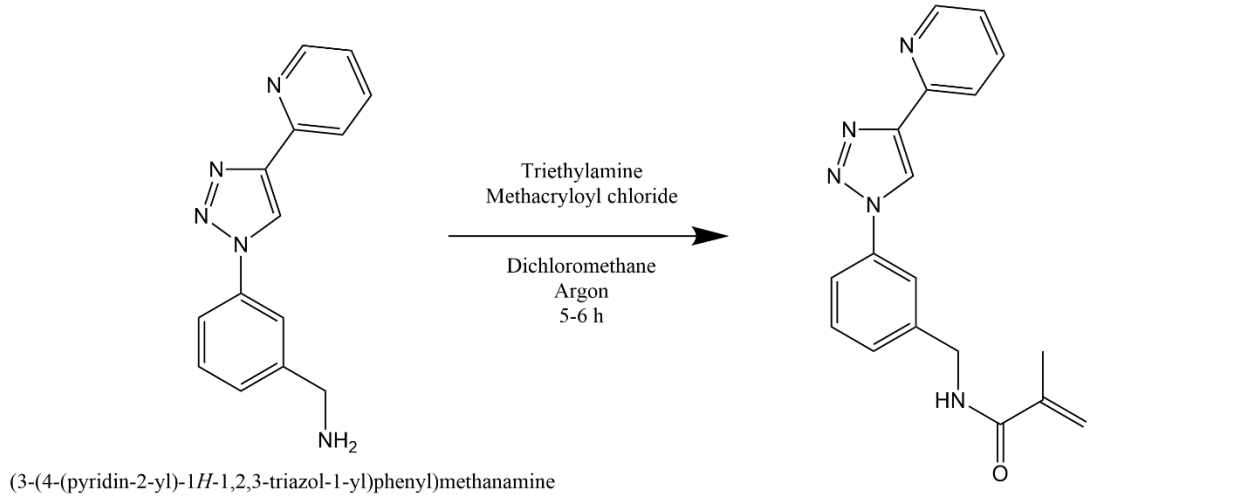

(3-(4-(pyridin-2-yl)-1*H*-1,2,3-triazol-1-yl)phenyl)methanamine
Chemical Formula: $C_{14}H_{13}N_5$

N-(3-(4-(pyridin-2-yl)-1*H*-1,2,3-triazol-1-yl)benzyl)methacrylamide
Chemical Formula: $C_{18}H_{17}N_5O$

Scheme 10: Schematic representation for the synthesis of Met-B2-A27.

Mass and NMR data

^{1}H (600 MHz; DMSO-D6): 1.96 (m, 1H, methyl), 4.65 (s, 2H, NH-CH2-aromatic), 5.56 (s, 1H, ethylene), 5.64 (s, 1H, ethylene), 7.23 (s, 2H, aromatic), 7.48 (s, 1H, aromatic), 7.62 (m, 2H, aromatic), 7.75 (m, 1H, aromatic), 7.83 (s, 1H, triazole), 8.27 (s, 1H, aromatic-triazole), 8.73 (s, 1H, aromatic-N), 8.89 (s, 1H, amide).

^{13}C (600 MHz; DMSO-D6): 18.7 (CH3, 1-alpha, C-C), 43.1 (CH2-NH2), 119.2 (CH2, ethylene), 120.1 (CH aromatic), 124.3 (CH aromatic), 126.9 (CH aromatic), 131.2 (CH triazole), 137.6 (Cq-N aromatic), 139.7 (Cq-C aromatic), 143.2 (C-ethylene), 148.3 (C-N aromatic), 150.5 (C-aromatic), 168.2 (C-amide).

ESI: M+1 = 320.1857.

Optimization of DNA extraction from a single capsule and NGS identification

Since individual hydrogel capsules contain unique genotypes from different HUVECs, extracting gDNA from each capsule is an essential first step to identifying each material's barcode. Cells are present within crosslinked hydrogel matrix, which makes it challenging to isolate cells from the hydrogel. Cell isolations and gDNA extraction steps were optimized to increase gDNA content by comparing lysis compositions, cell density, and extraction temperature (**Supplementary Fig. 4**). Pre-implant HUVECs capsules were used to compare DNA extraction efficiency in different conditions. First, each capsule was dissociated with EDTA solution. Lysis of capsules with EDTA before extracting DNA from a single capsule improved DNA extraction efficiency ~5-fold (**Supplementary Fig. 4a**). Also, flash-frozen capsules showed a similar DNA content level with fresh samples, confirming that explanted capsules can be stored for future use

after flash freezing steps. Also, different elution conditions were compared to increase the extracted DNA amount (**Supplementary Fig. 4b**). When samples were eluted with pre-warmed elution buffer at 56°C, DNA content was increased. In addition, as elution volume increased, the total DNA amount increased. However, increasing elution volume reduced DNA concentration, and 100 μl of elution buffer was chosen as the optimal volume for further analysis. Finally, cell numbers per capsule were adjusted by comparing different cell density conditions (**Supplementary Fig. 4c**). Extracted DNA content was elevated as cell density per capsule was increased. However, total DNA yield was decreased, so ~20,000 cells/capsule was set as the minimum cell density for encapsulation. The optimized conditions were applied to extract gDNA from explanted capsules, and these extracted gDNA samples were used for optimizing NGS methods.

Successful DNA extraction was done from *in vitro* and *in vivo* explanted capsules with high quality and enough human DNA content for polymerase chain reaction (PCR) amplification, followed by NGS for SNP genotyping. Furthermore, NGS library preparation was optimized to increase the on-target rate even with low DNA input (**Supplementary Fig. 5**). Finally, the bioinformatic pipeline shows the high-throughput strategy of the NGS analysis process for material/donor identification (**Supplementary Fig. 6**).

Optimization of donor barcoding and identification

We devised a new method that used a dual donor barcoding strategy to further increase the high-throughput screening ability and expand the combinatorial approach. By combining two different donors from 20 donors, a total of 400 donor pairs was created. First, to test the feasibility of mixed donors, the blend ratio of two donors was optimized *in vitro*. Three donor combinations (H15&H16, H16&H17, H15&H17) with three different blend ratios (1:2, 1:3, 1:4) were used for this study, and subsequently, a total of 9 different conditions were tested (**Supplementary Fig. 7a).** One capsule from each group was mixed, and the donor pairs of 9 capsules were analyzed (sample no. 1-9). Three different mixing ratios were tested to find the optimal condition with higher identification confidence (goodness levels). Log-likelihood analysis was applied to deconvolute donor identity. All samples were successfully identified with their matching donor pairs. The goodness level decreased as the cell density of the two mixing cells was more apart from one another. The blend ratio of donor1: donor2 was set to 1:2 as optimal conditions for further experiments (**Supplementary Fig. 7b-d**).

Next, with the optimized condition *in vitro*, the identification feasibility with three different materials was tested in mice. Three materials (Z1-A34: positive control mitigating FBRs, UP-VLVG: unmodified control, and B1-A51: a negative control unable to mitigate fibrosis) encapsulating two donor pairs at 1:2 ratios were prepared. The mixtures of three materials (20 capsules/material for each mouse) were implanted into IP space in mice (M1-M3) for two weeks (**Supplementary Fig. 8a-b**). After retrieving capsules (**Supplementary Fig. 8c**), they were separated into three groups based on fibrosis levels (**Supplementary Fig. 8d**). A total of 45 capsules were selected for donor identification, and the corresponding materials were determined

(**Supplementary Fig. 8e-f**). 43/45 (95.6%) of donor pairs were successfully identified among 400 donor combinations, suggesting that this mixed donor barcoding strategy can be applied to screen hundreds of materials in a larger animal model. The result of this cohort showed that previously published Z1-A34 (immune protective material) has the highest numbers of low fibrosis capsules, following UP-VLVG (unmodified alginate). The ability to screen hundreds of materials with this dual barcoding strategy will exponentially extend the high-throughput potential of the screening to identify materials mitigating FBRs.

Material characterization and evaluation of catheters coated with lead molecules.

XPS results showed higher nitrogen content in catheters coated with the small molecules than uncoated catheters, suggesting an effective attachment of nitrogen-containing small molecules to the catheters (**Fig. 6b**). Moreover, the Br^- content increase in bromine-containing Z1-A3 coated catheters supports the attachment of small molecules to the catheter surface. The XPS results were further supported by Tof-SIMS results showing higher CN^- content in catheters coated with small molecules and higher Br^- content in bromine-containing Z1-A3 coated catheters (**Fig. 6c, Supplementary Fig. 10a-b**) compared to uncoated ones. Additionally, the Met-Z1-A3 and Met-B2-A17 catheters appeared smoother than the unmodified catheter observed from the SEM images **(Supplementary Fig. 10c)**, possibly due to the removal of microscopic bumps during the coating process.

Supplementary Figures

Supplementary Figure 1. Schematic diagram for the synthesis of 211 alginate analogs.

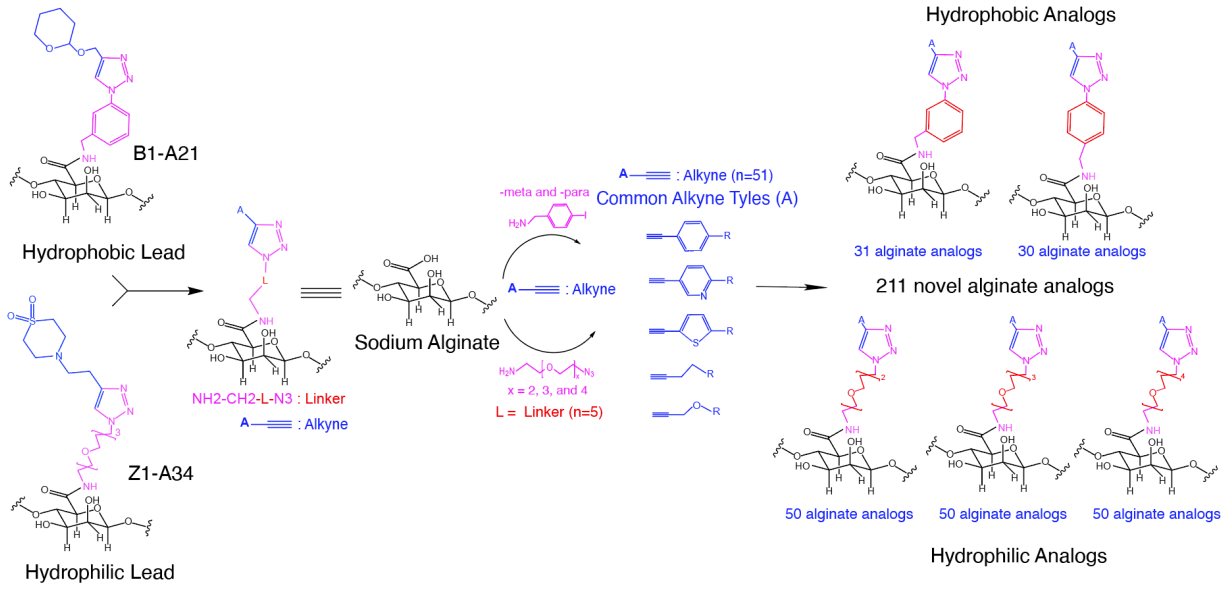

Supplementary Fig. 1) Schematic diagram for the synthesis of 211 alginate analogs. Left of the scheme are two of the previous triazole-containing lead alginates (B1-A21 and Z1-A34) that prevent fibrosis in mouse and NHP models. Total 211 new alginate analogs were synthesized by varying the lead hydrophilic linker (Azido PEG-amine) and hydrophobic linker (iodo benzyl amine) combined with a set of alkyne classes highlighted in blue colors.

Supplementary Figure 2. Material characterization.

a

Alginate-Linker		%C	%H	%N
Z2	Alginate-PEG2	37.19	5.03	7.37
Z1	Alginate-PEG3	35.86	5.41	7.64
Z4	Alginate-PEG4	39.24	5.52	8.15
B2	Alginate-3 ido Benzyle amine	37.1	5.35	4.05
B1	Alginate-4 ido Benzyle amine	37.13	5.25	2.35

b

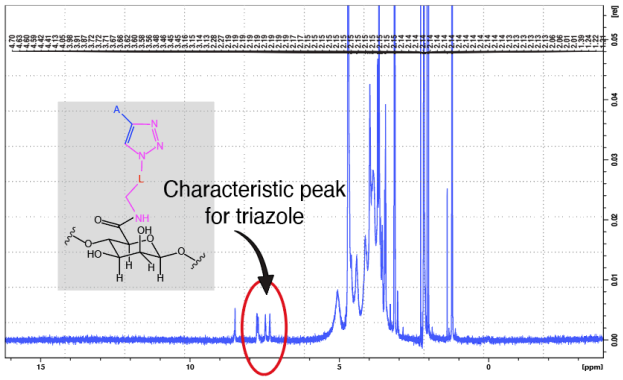

Supplementary Fig. 2) Material characterization. a, Table for elemental analysis of alginate linkers confirming the linker conjugation to the alginate backbone. **b**, Representative NMR image to show the triazole peak in alginate analogs confirming the modifications.

Supplementary Figure 3. Capsule optimization.

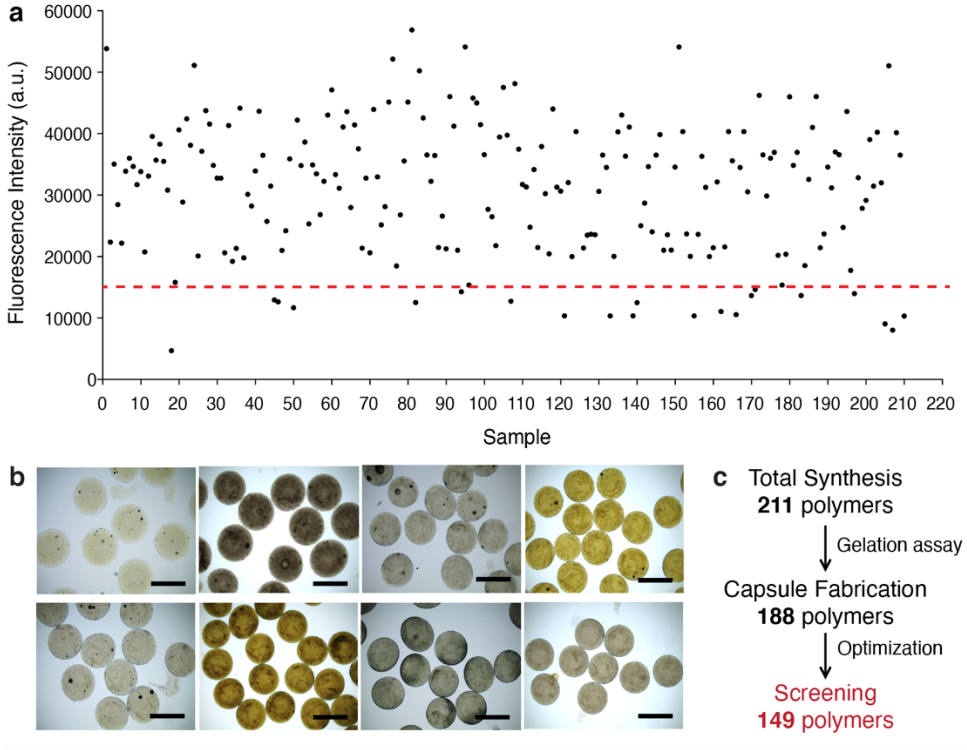

Supplementary Fig. 3) Capsule optimization. a, Gelation assay of alginate analogs using Rhodamine B entrapment. **b**, Representative images of capsule formation using the alginate analogs. Scale bar, 2mm. **c**, After initial characterization studies, including purity, solubility, and gel-forming ability, 149 alginate polymers were used for the screening test.

Supplementary Figure 4. Optimization of DNA extraction method with pre-implant capsules.

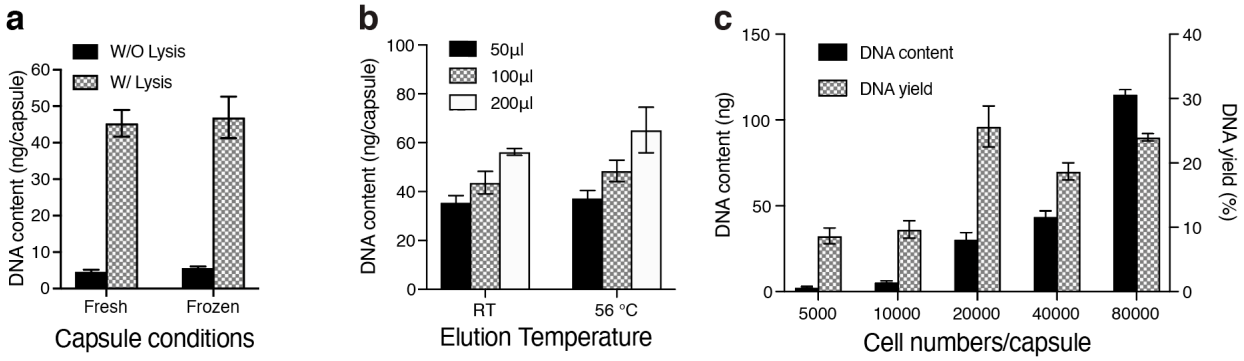

Supplementary Fig. 4) Optimization of DNA extraction method with pre-implant capsules. An optimized method was used for further analysis, such as qPCR and NGS identification with post-implant capsules. **a**, Comparison of DNA content depending on capsule lysis conditions; with vs. without EDTA lysis steps and fresh vs. frozen conditions. **b**, Comparison of DNA content depending on DNA elution conditions; elution volume and elution temperature. **c**, Comparison of DNA content/yield depending on cell numbers per capsule.

Supplementary Figure 5. Optimization of NGS library preparation workflow.

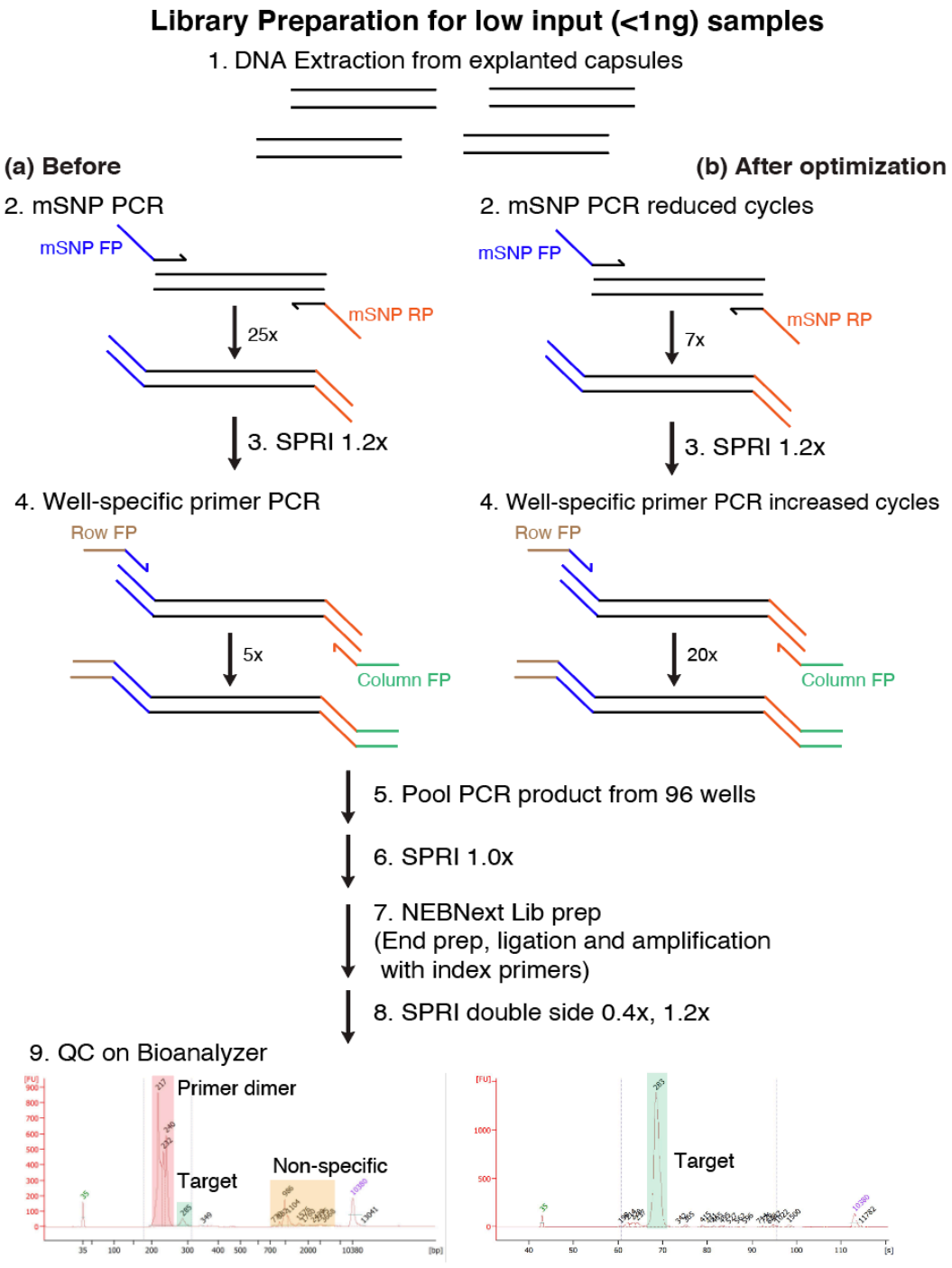

Supplementary Fig. 5) Optimization of NGS library preparation workflow. The library preparation involved a multiplex PCR step in amplifying the SNP loci, a barcoding PCR step to add position barcode to each sample, and a ligation-based sequencing adapter amendment procedure. **a**, Before optimization, the library on-target rate was <10%, with primer-dimers and non-specific PCR products contributing to the majority of reads. **b**, After optimization, the on-target rate was increased to >80% regardless of low DNA input (<1ng) in the starting material.

Supplementary Figure 6. Bioinformatic pipeline for determining material identity/composition from NGS sequencing data.

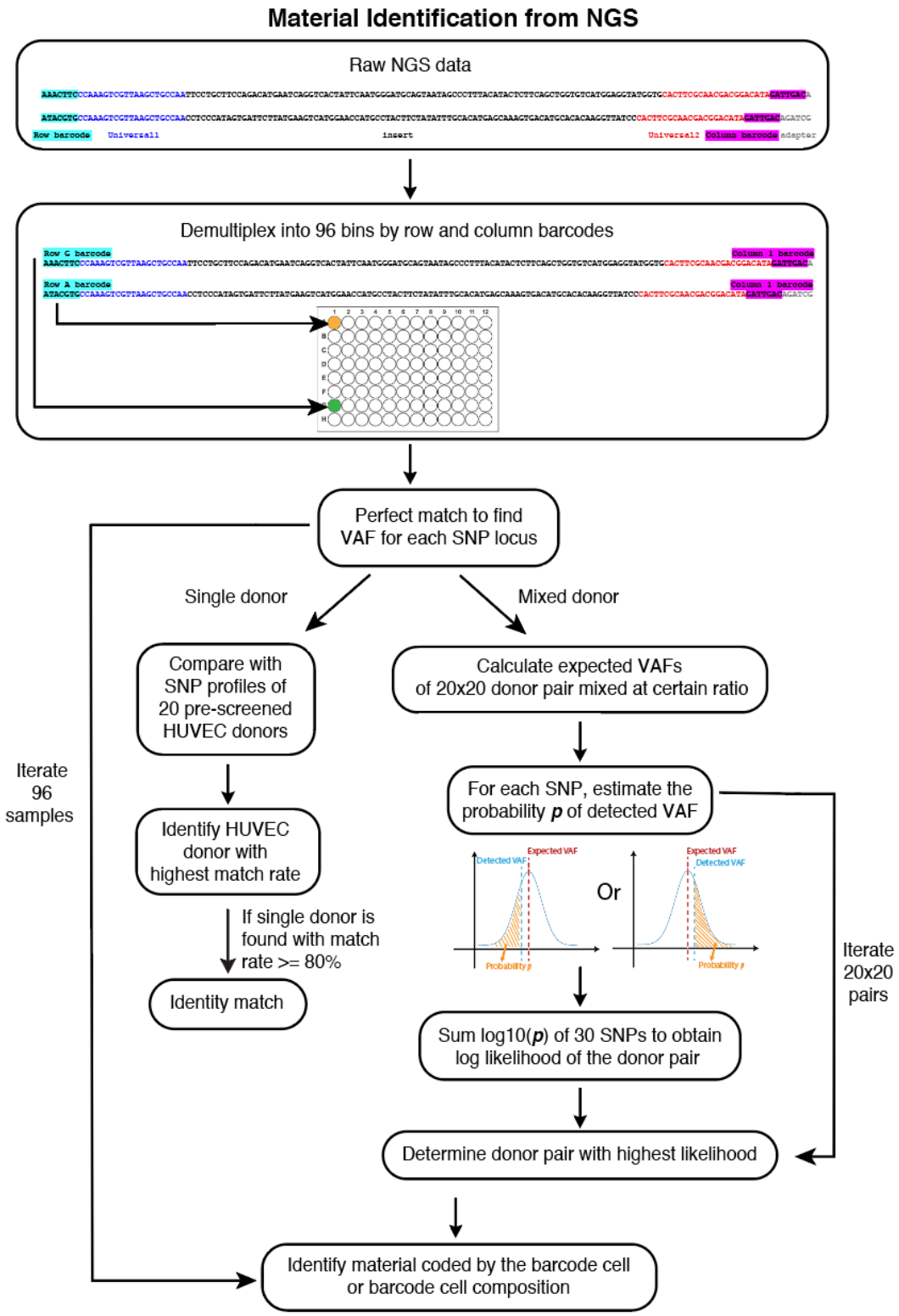

Supplementary Fig. 6) Bioinformatic pipeline for determining material identity/composition from NGS sequencing data. Fastq NGS data was demultiplexed by row and column barcodes to re-group sequences amplified from the same DNA input. Then for each amplicon sequence, the grep function was applied to search the dominant and variant alleles to calculate variant allele frequency (VAF) for each SNP locus. If the encapsulated cells comprised only one donor, the VAF profile was compared against profiles of the 20 pre-screened HUVEC donors. The donor with the highest match rate was identified as the encapsulated donor cell. When one or two donors were used as encapsulated cells, the log-likelihood of all possible donor compositions was calculated. The composition with the highest overall log-likelihood was determined as the cell composition (Quality control for log-likelihood analysis: 1) at least 25/30 SNP loci had sequencing coverage >50; and 2) overall log-likelihood higher than -200, and 3) goodness measurement higher than 10 where goodness is defined as the difference of log-likelihood between the most likely and the second most likely donor pairs). The material corresponding to the identified donor cell or cell composition would be the material encapsulating cells.

Supplementary Figure 7. Optimization of two HUVEC donors barcoding for expanded barcoding capacity for larger library screening.

a

Sample No.	Donor 1 20,000 cells/capsule	Donor 2 40,000 cells/capsule	Ratio Donor1: Donor2	Goodness
1	H17	H15	1:2	50.62
2	H17	H15	1:3	33.31
3	H17	H15	1:4	16.84
4	H16	H17	1:2	122.69
5	H16	H17	1:3	118.67
6	H16	H17	1:4	47.95
7	H16	H15	1:2	46.15
8	H16	H15	1:3	20.72
9	H16	H15	1:4	15.95

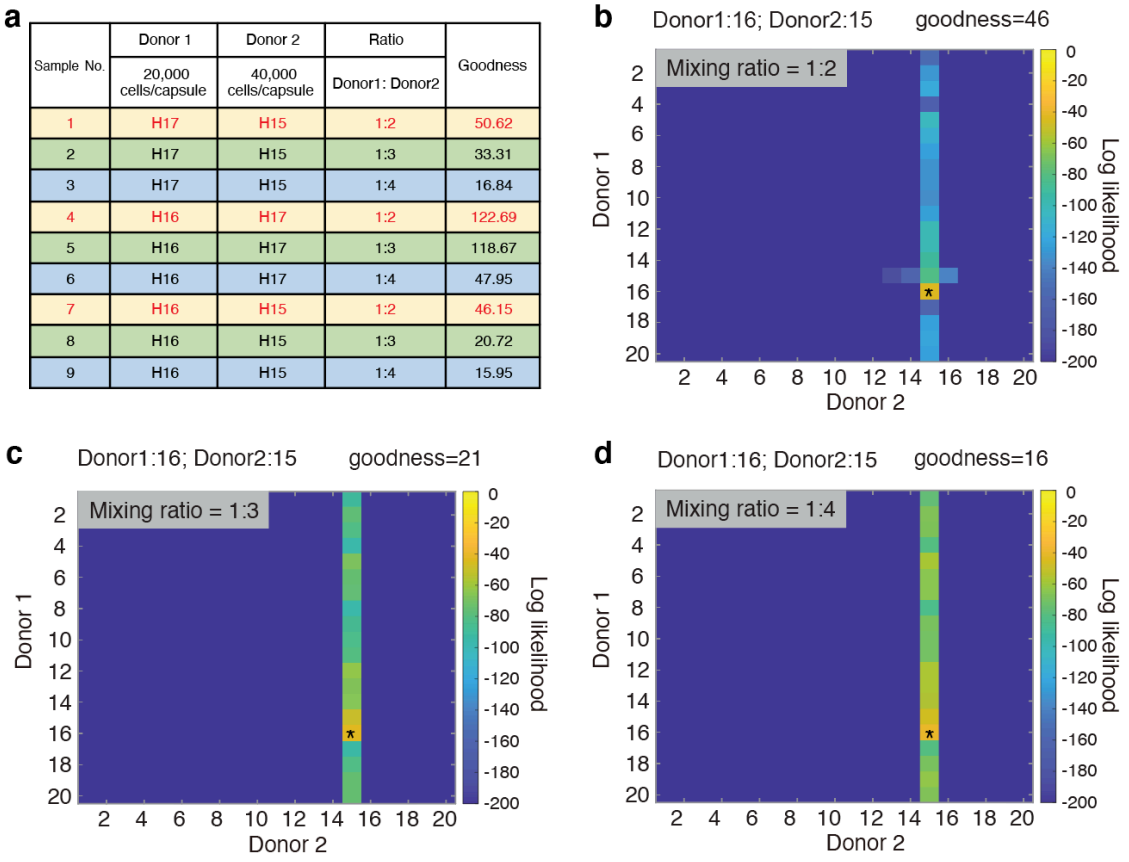

Supplementary Fig. 7) Optimization of two HUVEC donors barcoding for expanded barcoding capacity for larger library screening. a, Mixture of three different materials containing corresponding donor pairs were tested *in vitro*. Goodness is the log-likelihood difference between the picked most likely pair and the second most likely pair, which is a measurement of how stand-out is the picked combination. **b-d**, Representative heatmaps plot the log-likelihood of each 20x20 donor combination in different mixing ratios (**b**, 1:2, **c**, 1:3, **d**, 1:4). The color of each small square codes for the likelihood.

Supplementary Figure 8. Dual donor barcoding identification in C57BL/6J mice.

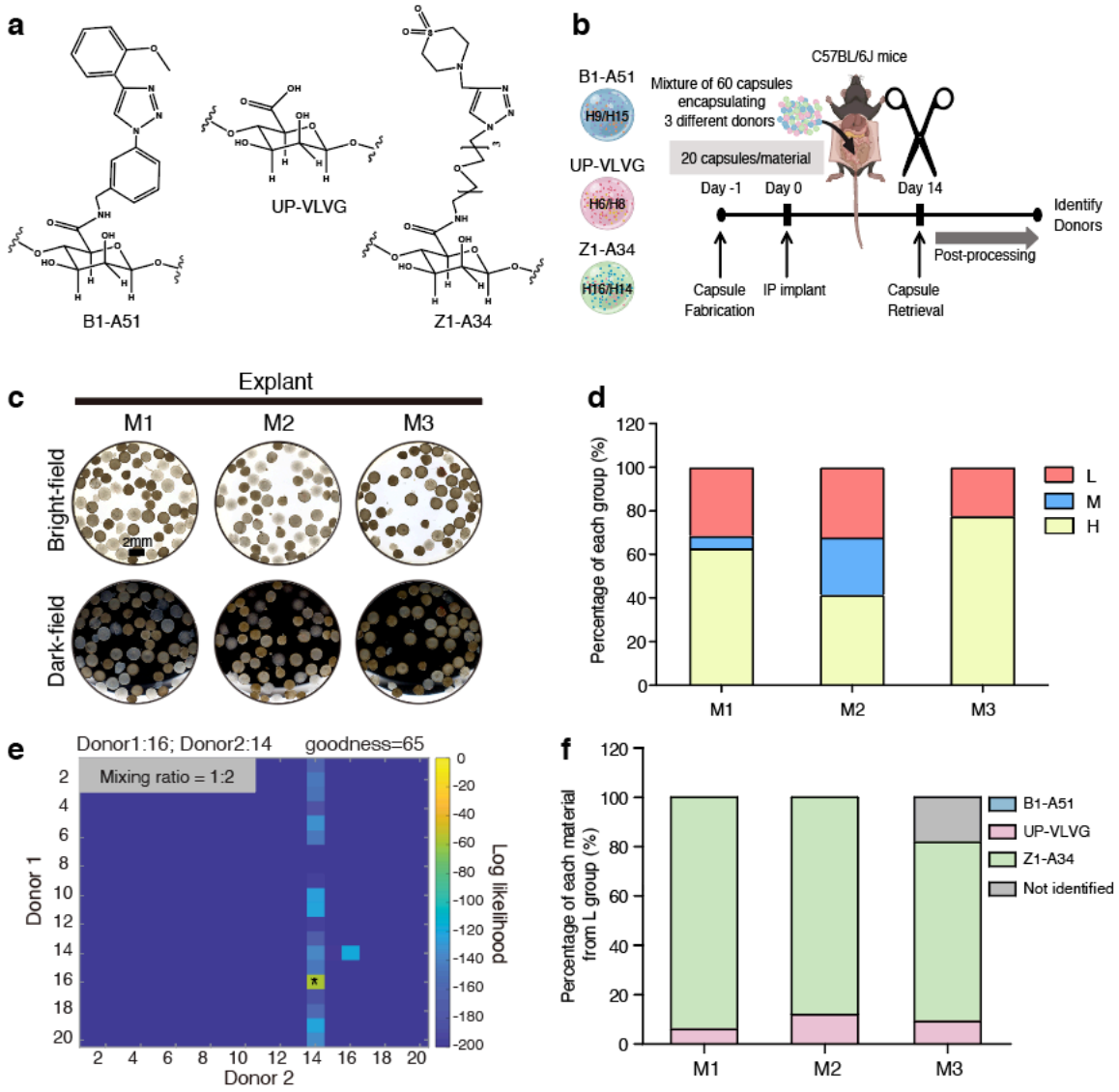

Supplementary Fig. 8) Dual donor barcoding identification in C57BL/6J mice. **a**, Three different materials were tested; UP-VLVG (control), B1-A51 (one of the negative materials), and Z1-A34 (one of the positive materials). **b**, Schematic workflow of three materials screening containing mixed dual donors. **c-d**, After two weeks of implant, capsules were retrieved from each mouse (M1-M3) and were separated into three groups depending on fibrosis levels. **e**, Representative heatmap result of identified donor pair. **f**, 39 mapped to Z1-A34 (positive control material), coded by H16:H14 at 1:2 ratio; 4 mapped to UP-VLVG coded by H6:H8 at 1:2 ratio; 0 sample mapped to B1-A51. Overalled 43/45 samples were mapped from the 400 donor SNP profile. Proportions of each material corresponded to donor pairs were plotted, and Z1-A34 showed the highest value indicating the best immune-protective properties.

Supplementary Figure 9. Diabetic reversal study with lead material (Z4-A10).

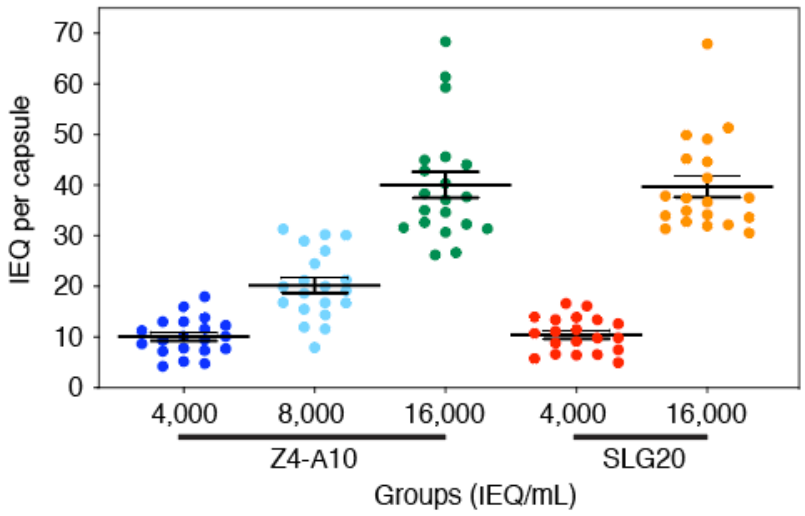

Supplementary Fig. 9) Diabetic reversal study with lead material. Capsules containing human islets were fabricated at final cell density with 4,000, 8,000, and 16,000 IEQ/alginate volume (mL). The final IEQ values in each capsule were 10, 20, and 40 IEQ per capsule, respectively. In each group, 500μL, 250μL, and 125μL of capsules were implanted in IP space, containing total 2,000 IEQ per mouse.

Supplementary Figure 10. Material characterization and evaluation of catheters coated with lead molecules.

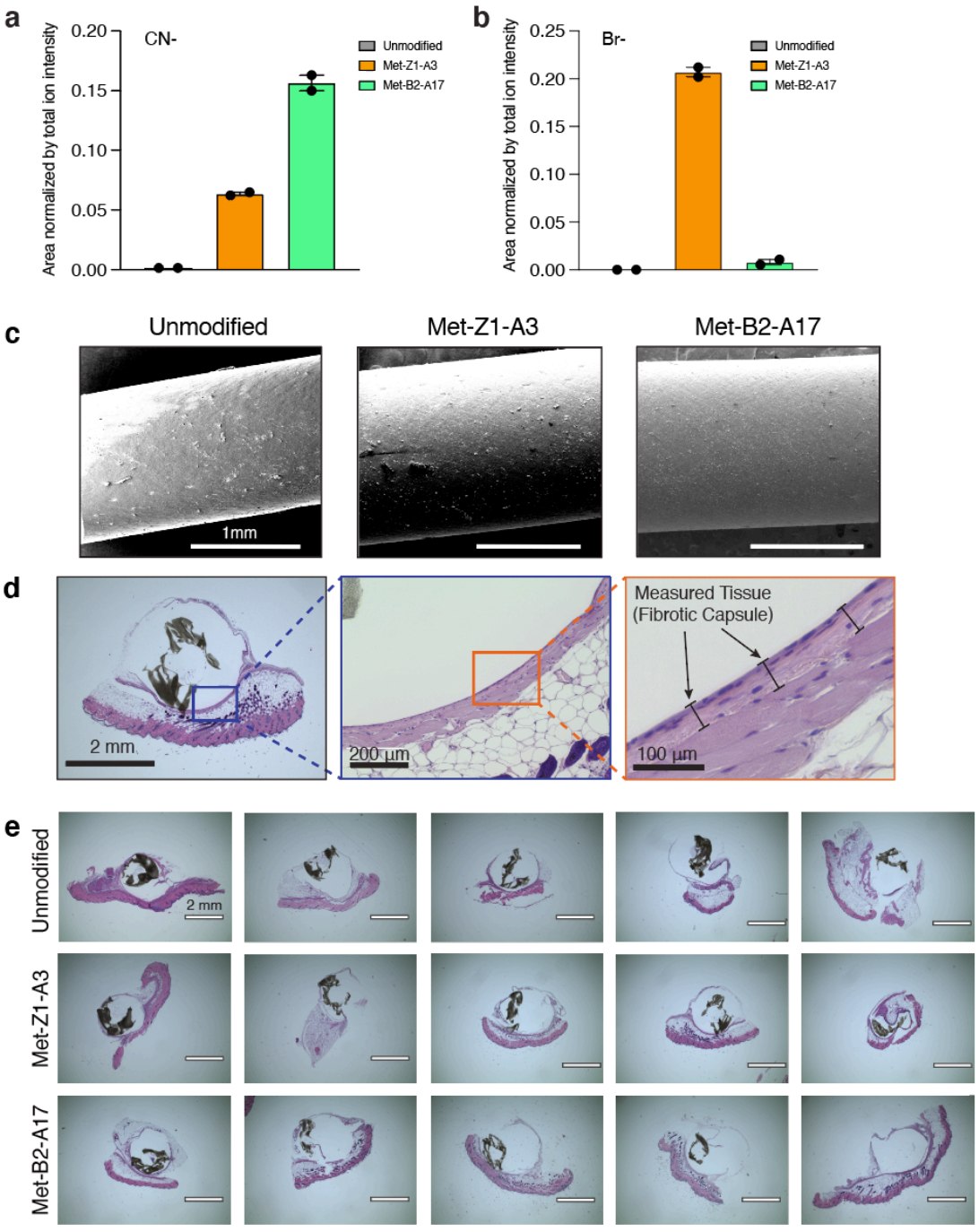

Supplementary Fig. 10) Material characterization and evaluation of catheters coated with lead molecules. a-b, The total intensity of two main peaks analyzed by Tof-SIMS (**a**, CN- and **b**, Br-) were plotted to compare with the unmodified catheter. **c**, Representative SEM images of unmodified and coated catheters. **d**, Example of the measured deposited fibrotic capsule tissue. ImageJ was used to measure tissue deposition via the purple band of tissue adjacent to the catheter. **e**, Representative H&E-stained sections for explanted catheters of each group. Scale bar, 2mm.

Supplementary Tables

Supplementary Table 1. Table of alginate formulations

Name	Company	Batch no.	Viscosity [mPa*s]	Usage
UP-VLVG	Novamatrix	BP-1903-04	<20	Starting material for alginate modification
SLG20		BP-1811-27	20 - 200	Control (Unmodified alginate)
SLG100		BP-1806-13	20 - 200	Blending material with modified alginate

Supplementary Table 2. Table of alkynes and linkers with notations.

Alkyne Table					Linker Table
A1 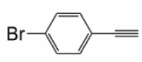	A11 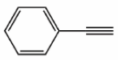	A21 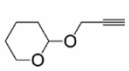	A31 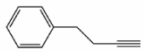	A41 	Z1 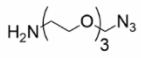
A2 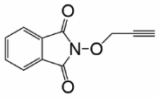	A12 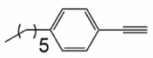	A22 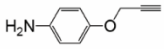	A32 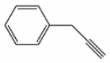	A42 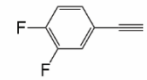	Z2 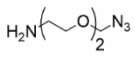
A3 	A13 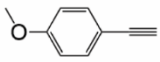	A23 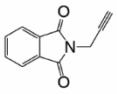	A33 	A43 	Z4 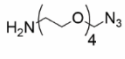
A4 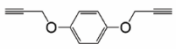	A14 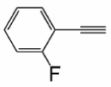	A24 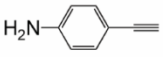	A34 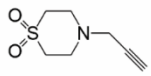	A44 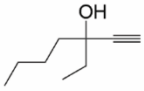	B1 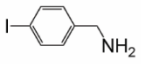
A5 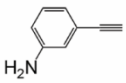	A15 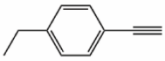	A25 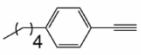	A35 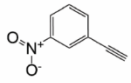	A45 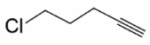	B2 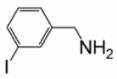
A6 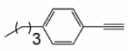	A16 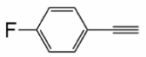	A26 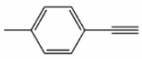	A36 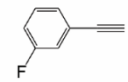	A46 	
A7 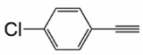	A17 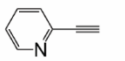	A27 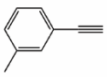	A37 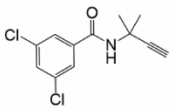	A47 	
A8	A18	A28	A38	A48	
A9	A19	A29	A39	A49	
A10	A20	A30	A40	A50	A51

Supplementary Table 3. 20 different HUVEC donor information

Donor Code	Cells	Company	Cat No.	Lot No.
H1	Human Umbilical Vein Endothelial Cells (HUVECs)	Lonza	CC-2517	0000260634
H2				0000315132
H3				0000315288
H4				0000317156
H5				0000317687
H6				18TL142763
H7				0000321046
H8				0000319181
H9				0000319180
H10				0000318930
H11				0000316669
H12				0000198228
H13				0000254439
H14				0000246600
H15				0000246083
H16				0000278143
H17				0000273864
H18				0000273863
H19				0000269280
H20				0000269279

Supplementary Table 4. Mouse screening results and rank orders.

Material. No.	Alginate Code	Material. No.	Alginate Code	Material. No.	Alginate Code	Material. No.	Alginate Code
1	UP-VLVG	41	B1-A31	81	Z1-A18	121	Z1-A21
2	Z4-A12	42	Z2-A30	82	Z1-A26	122	B2-A32
3	B2-A7	43	Z2-A38	83	Z1-A13	123	Z4-A17
4	B2-A12	44	Z4-A23	84	Z1-A49	124	Z2-A36
5	B2-A13	45	Z4-A7	85	Z1-A4	125	Z4-A26
6	Z1-A28	46	Z1-A9	86	Z2-A4	126	Z1-A30
7	Z2-A25	47	Z4-A32	87	Z2-A2	127	B2-A3
8	Z4-A6	48	Z4-A2	88	B2-A11	128	Z1-A5
9	B1-A15	49	B2-A29	89	Z1-A37	129	B2-A31
10	B1-A10	50	B2-A30	90	Z4-A34	130	Z2-A28
11	B1-A26	51	Z2-A22	91	Z1-A2	131	Z4-A9
12	Z1-A25	52	Z4-A20	92	Z2-A27	132	Z1-A7
13	Z1-A38	53	B2-A4	93	B2-A10	133	Z4-A27
14	Z4-A47	54	Z1-A1	94	Z2-A8	134	B2-A26
15	B1-A32	55	Z4-A28	95	Z4-A42	135	Z1-A34
16	B1-A12	56	Z4-A16	96	Z2-A21	136	B1-A34
17	B1-A36	57	Z4-A24	97	Z1-A47	137	Z4-A30
18	Z2-A31	58	Z1-A42	98	Z2-A3	138	Z1-A19
19	B1-A38	59	Z2-A26	99	Z2-A32	139	Z2-A20
20	Z4-A11	60	Z1-A10	100	B2-A9	140	Z1-A43
21	Z4-A13	61	Z1-A29	101	B2-A20	141	Z1-A17
22	Z2-A13	62	B2-A8	102	B2-A15	142	Z4-A43
23	Z2-A15	63	Z4-A31	103	B2-A22	143	Z4-A22
24	B1-A1	64	Z1-A23	104	B2-A34	144	B2-A17
25	B1-A5	65	Z4-A36	105	B2-A25	145	Z1-A14
26	B1-A23	66	Z4-A4	106	Z4-A21	146	Z1-A16
27	Z4-A46	67	Z4-A3	107	Z2-A18	147	Z1-A3
28	Z2-A40	68	B2-A19	108	B2-A23	148	Z2-A19
29	Z4-A8	69	B2-A27	109	Z4-A14	149	Z4-A10
30	B2-A21	70	Z4-A18	110	Z1-A27		
31	Z2-A14	71	Z4-A29	111	Z4-A1		
32	B2-A28	72	Z4-A44	112	Z4-A19		
33	Z1-A46	73	Z2-A37	113	Z1-A39		
34	Z1-A8	74	Z1-A31	114	Z2-A10		
35	Z4-A15	75	Z2-A23	115	Z1-A40		
36	Z2-A16	76	Z4-A35	116	Z1-A24		
37	Z2-A7	77	B2-A6	117	Z1-A15		
38	Z4-A25	78	Z1-A32	118	Z2-A35		
39	B2-A18	79	B2-A14	119	B2-A16		
40	Z2-A29	80	B2-A1	120	Z1-A44		

Supplementary Table 5. List of RT-qPCR primers.

Target	Primers (5'→3')
Mouse Alpha Smooth muscle actin (a-SMA)	Forward: CGCTTCCGCTGCCCAGAGACT
	Reverse: TATAGGTGGTTTCGTGGATGCCCGCT
Mouse Collagen 1a1 (Col1a1)	Forward: CATGTTCAGCTTTGTGGACCT
	Reverse: GCAGCTGACTTCAGGGATGT
Mouse b-actin (ActB)	Forward: GCTTCTTTGCAGCTCCTTCGTT
	Reverse: CGGAGCCGTTGTCGACGACC

Supplementary Table 6. SNP information and SNP primer sequences.

	SNP ID	Position (GrCh38)		Primer sequence (5'→3')
1	rs10230708	7:26625472	Forward	CCAAAGTCGTTAAGCTGCCAAACCAATGGGAGTCACTGCTG
			Reverse	TATGTCCGTCGTTGCGAAGTGCCTGGACATCAGTGTCCTCATCT
2	rs2043583	3:24598078	Forward	CCAAAGTCGTTAAGCTGCCAACCTGAATGTCAGTTTTGTTAGAGCAAC
			Reverse	TATGTCCGTCGTTGCGAAGTGACAGGGTGATGTAAAAGTGTCTGA
3	rs955456	4:23651593	Forward	CCAAAGTCGTTAAGCTGCCAACAGACTTAATCAAAGCCCTTGAAAAGA
			Reverse	TATGTCCGTCGTTGCGAAGTGACTCATGGCAACTTGCTTCTCA
4	rs966516	4:24775000	Forward	CCAAAGTCGTTAAGCTGCCAACCTCCCATAGTGATTCTTATGAAGTCA
			Reverse	TATGTCCGTCGTTGCGAAGTGGGATAACCTTGTGTGCATGTCACT
5	rs11247921	1:26339111	Forward	CCAAAGTCGTTAAGCTGCCAACCACACTCTGCCTCTCATGGTAT
			Reverse	TATGTCCGTCGTTGCGAAGTGAGGCAAGTAAGCAGACAATAGCA
6	rs10510620	3:29288795	Forward	CCAAAGTCGTTAAGCTGCCAATCCGCAAAACCTACAATCTCTGAA
			Reverse	TATGTCCGTCGTTGCGAAGTGCAGTATAGCTGAGGTAACCACAGTA
7	rs3789806	7:140749271	Forward	CCAAAGTCGTTAAGCTGCCAACTTGTATATAGACGGTAAAATAAACACCAAGA
			Reverse	TATGTCCGTCGTTGCGAAGTGCTGGACAGTTACCTTATTCAAACATCA
8	rs1884444	1:67168129	Forward	CCAAAGTCGTTAAGCTGCCAATTCCTGCTTCCAGACATGAATCA
			Reverse	TATGTCCGTCGTTGCGAAGTGCACCATACCTCCATGACACCA
9	rs16754	11:32396399	Forward	CCAAAGTCGTTAAGCTGCCAACTCTCTGCCTGCAGGATGTG
			Reverse	TATGTCCGTCGTTGCGAAGTGGCGTTTCTCACTGGTCTCAGAT
10	rs28932178	5:177210575	Forward	CCAAAGTCGTTAAGCTGCCAAACTAAGAGTGCAGAGCCTGGAA
			Reverse	TATGTCCGTCGTTGCGAAGTGTGGGGTTTGTGAACAAGAGTAGA
11	rs10741037	10:24041034	Forward	CCAAAGTCGTTAAGCTGCCAACACTTTATCAGACACAGTTATGTGCT
			Reverse	TATGTCCGTCGTTGCGAAGTGGCCCACATTTAGAATTTAGAGGTAACT
12	rs10805227	4:21513579	Forward	CCAAAGTCGTTAAGCTGCCAACTATCTGCAGGATTGTGTTCAATGTA
			Reverse	TATGTCCGTCGTTGCGAAGTGAGCAAACCACTGGGGAAAATACT
13	rs10833604	11:21712549	Forward	CCAAAGTCGTTAAGCTGCCAACTCTCTAGAGTGCAGATTGGTAGAA
			Reverse	TATGTCCGTCGTTGCGAAGTGCAAGTGAGAGACCAAGGAAAACAA
14	rs10964389	9:20022427	Forward	CCAAAGTCGTTAAGCTGCCAACAAAGTTGATAAATTAAAGGACTAAGGCAC

			Reverse	TATGTCCGTCGTTGCGAAGTGTTAAATCCTGCCTCTACTACTTGCT
15	rs11045749	12:21092846	Forward	CCAAAGTCGTTAAGCTGCCAACATTCTGTCTGGGATGAGGTGAT
			Reverse	TATGTCCGTCGTTGCGAAGTGAACAGTTATATGAAAAAAATGCTCAATATCACT
16	rs12213948	6:25424028	Forward	CCAAAGTCGTTAAGCTGCCAATGAAAGACGTCACAGCAAGGT
			Reverse	TATGTCCGTCGTTGCGAAGTGCGGGGACCAGGAGCAAAG
17	rs12259813	10:26967533	Forward	CCAAAGTCGTTAAGCTGCCAATGTAGGAGAGATTGGGCTAGAGAG
			Reverse	TATGTCCGTCGTTGCGAAGTGCTCTACCTGGGAAATCTCATTCATTC
18	rs1516755	11:21061449	Forward	CCAAAGTCGTTAAGCTGCCAACTAACTTCCTAACTAAAACTTTACAGTGGA
			Reverse	TATGTCCGTCGTTGCGAAGTGTCAGTAGAACTTTGAAGGGTACACA
19	rs1937037	9:22913892	Forward	CCAAAGTCGTTAAGCTGCCAAGCACGTAGATGAAATTGCCCCATA
			Reverse	TATGTCCGTCGTTGCGAAGTGACTTCCTACTTAGCCCTTTAGAAATGTAA
20	rs2616187	8:20811932	Forward	CCAAAGTCGTTAAGCTGCCAAGGAAAATATGTCTAAAAAGGCTCTGGAG
			Reverse	TATGTCCGTCGTTGCGAAGTGCCAGTGCAGTGTTTCTCAAACTC
21	rs2710998	7:24953942	Forward	CCAAAGTCGTTAAGCTGCCAAGTTTGTTCTAAGGTTCATCTGGTGAT
			Reverse	TATGTCCGTCGTTGCGAAGTGGCTCATGAAGAAAATAATCCTTATGGTAATC
22	rs2874755	8:27010387	Forward	CCAAAGTCGTTAAGCTGCCAATGTCCCACTTTTTACCTCCCTTC
			Reverse	TATGTCCGTCGTTGCGAAGTGCTTCATGGAGGAGATAGTAACTAAGGT
23	rs4665582	2:23290086	Forward	CCAAAGTCGTTAAGCTGCCAATGTGCTACGACAGAGCTAAGTAC
			Reverse	TATGTCCGTCGTTGCGAAGTGTGGTCAGCTTAAATAGCTACTGCT
24	rs4712476	6:20291800	Forward	CCAAAGTCGTTAAGCTGCCAACCCCGGATGTCAGGGAATG
			Reverse	TATGTCCGTCGTTGCGAAGTGGTGAGTATGCACGTCTCCATCT
25	rs611628	1:41832653	Forward	CCAAAGTCGTTAAGCTGCCAACCAGGCACCACTGCTTTGT
			Reverse	TATGTCCGTCGTTGCGAAGTGGCAAGGGGACAGAAATTTGCTTATC
26	rs7893462	10:27939936	Forward	CCAAAGTCGTTAAGCTGCCAAACCTTGTCAAGAACCTAAATAGTGAGAA
			Reverse	TATGTCCGTCGTTGCGAAGTGTGGGAGAGTTCACTGCACCT
27	rs7902135	10:25287563	Forward	CCAAAGTCGTTAAGCTGCCAACGTGGGCTAGTCAAGAATATAAAATGTTAG
			Reverse	TATGTCCGTCGTTGCGAAGTGCATGCAGGTGGTGTGAATCTC
28	rs9466930	6:23840904	Forward	CCAAAGTCGTTAAGCTGCCAATGTGTGGCTCAGTATACCACTTAG
			Reverse	TATGTCCGTCGTTGCGAAGTGCTCAAGCCATGTCATATTTTCAAATAGAC
29	rs2862909	13:24527029	Forward	CCAAAGTCGTTAAGCTGCCAAGCACATCATACATTATTTCTGTTGCTAT
			Reverse	TATGTCCGTCGTTGCGAAGTGAGAGCCCACTTAGCATCTCCA
30	rs1338945	20:23119232	Forward	CCAAAGTCGTTAAGCTGCCAAGAAATATTGCTGGGGTCAGCG
			Reverse	TATGTCCGTCGTTGCGAAGTGGGAGGGTTTAAGGTGTTTTATGTTTTG

Supplementary Table 7. Position barcoding primer sequences.

Primer Name	Primer Sequence (5'→3')
FP-R1	ATACGTGCCAAAGTCGTTAAGCTGCCAA
FP-R2	TGAAGTTCCAAAGTCGTTAAGCTGCCAA
FP-R3	TGATTAGCCAAAGTCGTTAAGCTGCCAA
FP-R4	CTAATCACCAAAGTCGTTAAGCTGCCAA
FP-R5	ATGACGCCCAAAGTCGTTAAGCTGCCAA
FP-R6	GTAATGTCCAAAGTCGTTAAGCTGCCAA
FP-R7	AAACTTCCCAAAGTCGTTAAGCTGCCAA
FP-R8	TCCGAGACCAAAGTCGTTAAGCTGCCAA
RP-C1	GTCAATCTATGTCCGTCGTTGCGAAGTG
RP-C2	CGCTATGTATGTCCGTCGTTGCGAAGTG
RP-C3	ACCGATTTATGTCCGTCGTTGCGAAGTG
RP-C4	AACACCGTATGTCCGTCGTTGCGAAGTG
RP-C5	CTCGGAATATGTCCGTCGTTGCGAAGTG
RP-C6	GACTGATTATGTCCGTCGTTGCGAAGTG
RP-C7	TACTGCGTATGTCCGTCGTTGCGAAGTG
RP-C8	AACTGGCTATGTCCGTCGTTGCGAAGTG
RP-C9	ATCGGTCTATGTCCGTCGTTGCGAAGTG
RP-C10	GCCAGTTTATGTCCGTCGTTGCGAAGTG
RP-C11	CACGTATTATGTCCGTCGTTGCGAAGTG
RP-C12	CGCATGTTATGTCCGTCGTTGCGAAGTG